Asteroid 21 Lutetia: Low Mass, High Density

M. Pätzold,[1]* T. P. Andert,[2] S. W. Asmar,[3] J. D. Anderson,[3] J.-P. Barriot,[4] M. K. Bird,[1,5] B. Häusler,[2] M. Hahn,[1] S. Tellmann,[1] H. Sierks,[6] P. Lamy,[7] B. P. Weiss[8]

Asteroid 21 Lutetia was approached by the Rosetta spacecraft on 10 July 2010. The additional Doppler shift of the spacecraft radio signals imposed by 21 Lutetia's gravitational perturbation on the flyby trajectory were used to determine the mass of the asteroid. Calibrating and correcting for all Doppler contributions not associated with Lutetia, a least-squares fit to the residual frequency observations from 4 hours before to 6 hours after closest approach yields a mass of (1.700 ± 0.017) × 10^{18} kilograms. Using the volume model of Lutetia determined by the Rosetta Optical, Spectroscopic, and Infrared Remote Imaging System (OSIRIS) camera, the bulk density, an important parameter for clues to its composition and interior, is (3.4 ± 0.3) × 10^3 kilograms per cubic meter.

Asteroid 21 Lutetia, discovered in 1852, is one of the larger main-belt asteroids. In 2004, it became the flyby target asteroid for the Rosetta spacecraft mission. An important characteristic of an asteroid is its bulk density, derived from its mass and its volume. Although there are a number of asteroid mass determination techniques, by far the most accurate is spacecraft tracking during a close flyby.

The velocity of a spacecraft flying by a body of sufficient size and at a sufficiently close distance is perturbed by the attracting force of that body. The perturbed velocity is estimated from the additional Doppler shift of the transmitted radio signal in comparison with the expected Doppler shift of an unperturbed trajectory (*1*).

The Rosetta spacecraft was tracked during the flyby of asteroid 21 Lutetia on 10 July 2010 with NASA's Deep Space Network (DSN) 70-m antenna (DSS-63) near Madrid, Spain (*2*). The flyby distance was d = 3168 ± 7.5 km, the high relative flyby velocity was v_0 = 14.99 km/s, and the projection angle between the relative velocity and the direction to Earth was α = 171.2°, all of which define the postencounter amplitude of the Doppler shift (*3*).

After correcting for contributions not associated with 21 Lutetia (*2*), the final Doppler frequency shift 6 hours after Rosetta's closest approach to the asteroid was Δf = 36.2 ± 0.2 mHz (Fig. 1). The value of GM (gravitational constant G × body mass M) from a least-squares fitting procedure is $GM = (11.34 \pm 0.11) \times 10^{-2}$ km^{3}s^{-2}, corresponding to a mass of (1.700 ± 0.017) × 10^{18} kg (error, 1.0%). The uncertainty in GM (*2*) considers the error from the least-squares fit mainly driven by the frequency noise (0.55%), the uncertainty in the 21 Lutetia ephemeris introduced by the uncertainty in the flyby distance of ±7.5 km (0.24%), and the considered uncertainty in the tropospheric correction introduced by the zenith delay model and the mapping function of the ground station elevation (0.8%). These contributions yield a total uncertainty of 1.0%. The values for GM and Δf agree within the error with the analytical solution (*3*). The derived mass is lower than other mass determinations of Lutetia from astrometry (fig. S7).

One of the most important global geophysical parameters—which provides clues to the origin, internal structure, and composition of 21 Lutetia—is its mean (bulk) density, derived from the mass and the volume. Observations of the Optical, Spectroscopic, and Infrared Remote Imaging System (OSIRIS) camera and ground observations using adaptive optics were combined to model the global shape. The derived volume is (5.0 ± 0.4) × 10^{14} m^3 (*4*). The volume leads to a bulk density of (3.4 ± 0.3) × 10^3 kg/m^3. This high bulk density is unexpected in view of the low value of the measured mass. It is one of the highest bulk densities known for asteroids (*5*). Assuming that Lutetia has a modest macroporosity of 12%, it would imply that the bulk density of its material constituents would exceed that of stony meteorites. Unless Lutetia has anomalously low porosity compared with other asteroids in its size range, its high density likely indicates a nonchondritic bulk composition enriched in high atomic number like iron. It may also be evidence for a partial differentiation of the asteroid body (*6*).

[1]Rheinisches Institut für Umweltforschung, Abteilung Planetenforschung, an der Universität zu Köln, 50931 Cologne, Germany. [2]Institut für Raumfahrttechnik, Universität der Bundeswehr München, 85579 Neubiberg, Germany. [3]Jet Propulsion Laboratory, California Institute of Technology, Pasadena, CA 91125, USA. [4]Géosciences du Pacifique Sud, Université de la Polynésie Française, BP 6570, 98702 Faa'a, Tahiti, Polynésie Francaise. [5]Argelander Institut für Astronomie, Universität Bonn, 53121 Bonn, Germany. [6]Max-Planck-Institut für Sonnensystemforschung, 37191 Katlenburg-Lindau, Germany. [7]Laboratoire d'Astrophysique de Marseille, Marseille, France. [8]Department of Earth, Atmospheric and Planetary Sciences, Massachusetts Institute of Technology, Cambridge, MA 02139, USA.

*To whom correspondence should be addressed. E-mail: martin.paetzold@uni-koeln.de

References and Notes

1. T. P. Andert *et al.*, *Geophys. Res. Lett.* **37**, L09202 (2010).
2. Materials and methods are available as supporting material on *Science* Online.
3. As shown in (*7*), the expected final postencounter Doppler shift of a two-way radio carrier signal is $\Delta f(t \rightarrow \infty) = 4 \frac{f_X}{c} \frac{GM}{d \cdot v_0} \cdot \sin\alpha' \cos\beta$, where α′ = 172.18° is the direction to Earth projected into the flyby plane and β = 3° is the direction angle to Earth above the flyby plane. Using the fit solution for Lutetia of $GM = (11.34 \pm 0.11) \times 10^{-2}$ km^3/s^2, the analytical result of the relation above is 36.4 ± 0.4 mHz.
4. H. Sierks *et al.*, *Science* **334**, 487 (2011).
5. Similar high bulk densities are known for the asteroids 4 Vesta, 16 Psyche, 20 Massalia, and 22 Kalliope, all

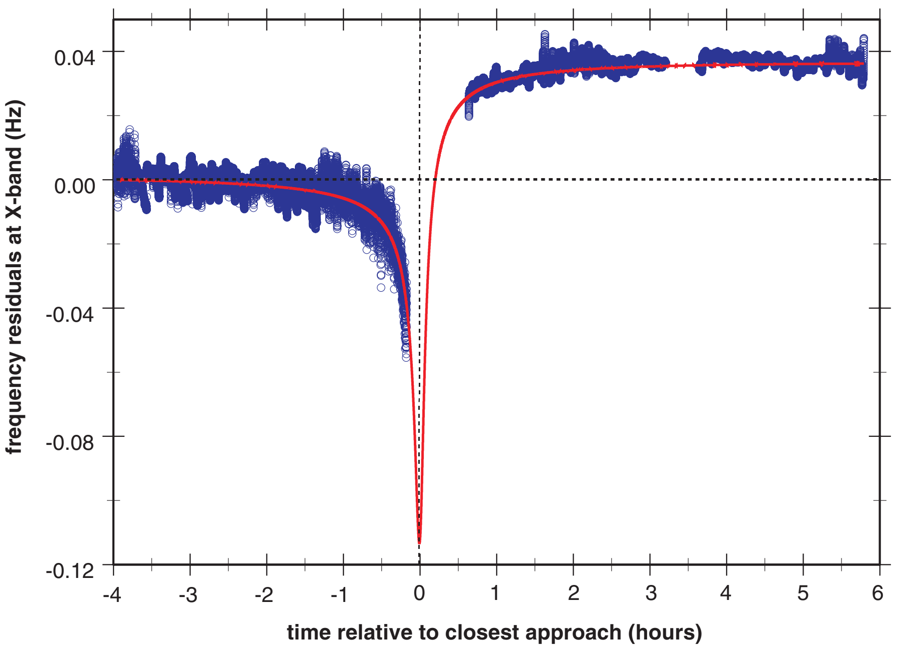

Fig. 1. Filtered and adjusted frequency residuals at X-band frequency from 4 hours before closest approach to 6 hours after closest approach. Two tracking gaps (light red shaded zones) are indicated from 5 min before closest approach to 45 min after closest approach as planned (*7*), and from 192 min to 218 min after closest approach when DSS 63 accidentally dropped the uplink. The red solid line is a least-squares fit to the data from which GM is determined.

of which are larger than Lutetia (*8*). Bulk densities of more primitive C-type asteroids are in the range 1200 kg/m^3 to 2700 kg/m^3.
6. B. P. Weiss *et al*., Evidence for thermal metamorphism or partial differentiation of asteroid 21 Lutetia from Rosetta, paper no. 2077, 42nd Lunar and Planetary Science Conference, The Woodlands, TX, 7 to 11 March 2011.
7. M. Pätzold *et al*., *Astron. Astrophys.* **518**, L156 (2010).
8. J. Baer, S. R. Chesley, R. D. Matson, *Astron. J.* **141**, 143 (2011).

Acknowledgments: The Rosetta Radio Science Investigation experiment is funded by the Deutsches Zentrum für Luft- und Raumfahrt (DLR), Bonn under grants 50QM1002 (T.P.A. and B.H.) and 50QM1004 (M.P., M.H., S.T., and M.K.B.), and under a contract with NASA (S.W.A. and J.D.A.). We thank T. Morley for valuable comments and all persons involved in Rosetta at the European Space Research and Technology Centre, European Space Operations Centre, European Space Astronomy Centre, Jet Propulsion Laboratory, and the European Space Tracking Network and Deep Space Network ground stations for their continuous support.

Supporting Online Material
www.sciencemag.org/cgi/content/full/334/6055/491/DC1
Materials and Methods
Figs. S1 to S7
References (*9*–*26*)

16 February 2011; accepted 4 October 2011
10.1126/science.1209389

The Surface Composition and Temperature of Asteroid 21 Lutetia As Observed by Rosetta/VIRTIS

A. Coradini,[1] F. Capaccioni,[2]* S. Erard,[3] G. Arnold,[4] M. C. De Sanctis,[2] G. Filacchione,[2] F. Tosi,[1] M. A. Barucci,[3] M. T. Capria,[2] E. Ammannito,[1] D. Grassi,[1] G. Piccioni,[2] S. Giuppi,[1] G. Bellucci,[1] J. Benkhoff,[5] J. P. Bibring,[6] A. Blanco,[13] M. Blecka,[7] D. Bockelee-Morvan,[3] F. Carraro,[1] R. Carlson,[8] U. Carsenty,[9] P. Cerroni,[2] L. Colangeli,[5] M. Combes,[3] M. Combi,[10] J. Crovisier,[3] P. Drossart,[3] E. T. Encrenaz,[3] C. Federico,[11] U. Fink,[12] S. Fonti,[13] L. Giacomini,[1] W. H. Ip,[14] R. Jaumann,[9] E. Kuehrt,[9] Y. Langevin,[6] G. Magni,[2] T. McCord,[15] V. Mennella,[19] S. Mottola,[9] G. Neukum,[16] V. Orofino,[13] P. Palumbo,[21] U. Schade,[22] B. Schmitt,[17] F. Taylor,[20] D. Tiphene,[3] G. Tozzi[18]

The Visible, InfraRed, and Thermal Imaging Spectrometer (VIRTIS) on Rosetta obtained hyperspectral images, spectral reflectance maps, and temperature maps of the asteroid 21 Lutetia. No absorption features, of either silicates or hydrated minerals, have been detected across the observed area in the spectral range from 0.4 to 3.5 micrometers. The surface temperature reaches a maximum value of 245 kelvin and correlates well with topographic features. The thermal inertia is in the range from 20 to 30 joules meter^{-2} kelvin^{-1} second$^{-0.5}$, comparable to a lunarlike powdery regolith. Spectral signatures of surface alteration, resulting from space weathering, seem to be missing. Lutetia is likely a remnant of the primordial planetesimal population, unaltered by differentiation processes and composed of chondritic materials of enstatitic or carbonaceous origin, dominated by iron-poor minerals that have not suffered aqueous alteration.

The visible, InfraRed, and Thermal Imaging Spectrometer (VIRTIS) on board the Rosetta spacecraft is an imaging and high-resolution spectrometer with two independent channels: VIRTIS-M, which acquires hyperspectral images in the spectral range from 0.25 to 5.1 μm with a spatial resolution of 250 μrad, and VIRTIS-H, a high-resolution infrared spectrometer in the 2- to 5-μm range with spectral resolution as high as 3000 (*1*–*3*).

VIRTIS-M obtained hyperspectral images of asteroid 21 Lutetia with spatial resolution varying between 12 km and less than 1 km, at closest approach. VIRTIS-H was operated throughout the flyby [supporting online material (SOM)]. Because of the orientation of the Lutetia spin axis, only about 50% of the surface has been imaged, ranging in latitude from the north pole down to the equator according to the OSIRIS shape model (*4*).

VIRTIS observed Lutetia at zero phase angle (0.007°), located at northern latitude 16.0° and east longitude 358.3°. The measured radiance factor (I/F, where I is the calibrated radiance and F is the solar flux) at zero phase is 0.21 ± 0.01 at 550 nm, consistent with the value measured by OSIRIS (*5*).

The full-disk spectra (Fig. 1) show a variability limited to within 3% shortward of 3.5 μm. Beyond 3.5 μm, the surface thermal emission becomes more and more relevant, and the spectral variations reflect the local time changes, from sunset to sunrise, and the corresponding surface temperature changes.

The VIRTIS-M spectra show no absorption features in the range from 0.5 to 2.5 μm to an rms level of less than 5% (Figs. 1 and 2), thus confirming previous disk-integrated ground-based observations (*6*, *7*). Asteroid 21 Lutetia has a moderately red slope in the range of 0.5 to 0.8 μm, whereas in the region of 0.8 to 2.5 μm the spectrum is essentially flat. Both VIRTIS-M and VIRTIS-H consistently did not identify any spectral feature associated with OH absorptions. In particular, VIRTIS-H, within its calibration accuracy of 2%, did not identify hydrated minerals bands at 1.9, 2.7, and 3 μm, thus ruling out their presence on the explored surface (SOM). VIRTIS did not identify any spectral features associated with organic materials in the 3.3- to 3.6-μm range.

Analysis of the normalized spectral variation across the observed surface at highest resolution and over a wide range of phase angles shows a remarkable uniformity of the surface spectral properties, showing a maximum fluctuation of 3%. This implies that any albedo variation would be related to regolith transport and/or sorting processes rather than compositional variation (Fig. 3A).

The region between 3.5 and 5.1 μm is dominated by the presence of the thermal emission of the asteroid's surface, from which we evaluated the surface temperature and the spectral emissivity. The temperature observed varied between 170 and 245 K, with a direct correlation of the temperature with topographic features and with maximum temperatures obtained for the smaller incidence angles on the left-hand side of the image (Fig. 3B).

We have applied a thermophysical model of the heat conduction into the asteroid surface derived from cometary nucleus evolution models (*8*). The model was used to fit the measured surface temperatures as a function of the density, specific heat, and thermal conductivity, assumed similar to those of a lunar regolith (*9*–*11*). A self-heating parameter (*12*) accounts for the contribution of unresolved topography and microroughness. Iteratively, we optimized the result-

[1]Istituto di Fisica dello Spazio Interplanetario, Istituto Nazionale di Astrofisica (INAF), 00133 Rome, Italy. [2]Istituto di Astrofisica Spaziale e Fisica Cosmica, INAF, 00133 Rome, Italy. [3]Laboratoire d'etudes spatiales et d'instrumentation en astrophysique (LESIA), Observatoire de Paris, CNRS, Université Pierre et Marie Curie, Université Paris-Diderot, 92195 Meudon, France. [4]Institute for Planetology, 48149 Münster, Germany. [5]European Space Research and Technology Centre (ESTEC), European Space Agency, 2200 AG Noordwijk, Netherlands. [6]Institut d'Astrophysique Spatial, CNRS, 91405 Orsay, France. [7]Space Research Center, Polish Academy of Sciences, 00-716 Warsaw, Poland. [8]Jet Propulsion Laboratory, National Aeronautics and Space Administration, Pasadena, CA 91109, USA. [9]Institute of Planetary Research, Deutsches Zentrum für Luft- und Raumfahrt (DLR), 12489 Berlin, Germany. [10]Department of Atmospheric, Oceanic and Space Sciences, The University of Michigan, Ann Arbor, MI 48109, USA. [11]Università di Perugia, 06100 Perugia, Italy. [12]Lunar Planetary Laboratory, University of Arizona, Tucson, AZ 85721, USA. [13]Dipartimento di Fisica, Università di Lecce, 73100 Lecce, Italy. [14]National Central University, Taipei, Taiwan. [15]Bear Fight Institute, Winthrop, WA 98862, USA. [16]Freie Universität, 14195 Berlin, Germany. [17]Université Joseph Fourier–Grenoble 1/CNRS-INSU, Institut de Planétologie et d'Astrophysique de Grenoble, 38041 Grenoble, France. [18]Osservatorio Astrofisico di Arcetri, 50125 Firenze, Italy. [19]Osservatorio di Capodimonte, 80131 Napoli, Italy. [20]Department of Physics, Oxford University, Oxford OX1 2JD, UK. [21]Università degli studi di Napoli "Parthenope," 80133 Napoli, Italy. [22]Helmholtz-Zentrum Berlin für Materialien und Energie, 14109 Berlin, Germany.

*To whom correspondence should be addressed. E-mail: fabrizio.capaccioni@inaf.it

www.sciencemag.org/cgi/content/full/334/6055/491/DC1

Supporting Online Material for

Asteroid 21 Lutetia: Low Mass, High Density

M. Pätzold, T. P. Andert, S. W. Asmar, J. D. Anderson, J.-P. Barriot, M. K. Bird, B. Häusler, M. Hahn, S. Tellmann, H. Sierks, P. Lamy, B. P. Weiss

*To whom correspondence should be addressed. E-mail: Martin.Paetzold@uni-koeln.de

Published 28 October 2011, *Science* **334**, 491 (2011)
DOI: 10.1126/science.1209389

This PDF file includes:

Materials and Methods
Figs. S1 to S7
References

Asteroid (21) Lutetia was approached by the Rosetta spacecraft on 10 July 2010. The additional Doppler shift of the spacecraft radio signals imposed by (21) Lutetia's gravitational perturbation on the flyby trajectory were used to determine the mass of the asteroid. Calibrating and correcting for all Doppler contributions not associated with Lutetia, a least-squares fit to the residual frequency observations from four hours before to six hours after closest approach yields a mass of (1.700 +/- 0.017)·10^{18} kg (error: 1.0%). Using the volume model of Lutetia determined by the Rosetta OSIRIS camera, the bulk density, an important parameter for clues to its composition and interior, is (3.4 +/- 0.3)·10^3 kg/m^3.

1. Flyby and Observation

The Rosetta spacecraft was tracked during the flyby at asteroid (21) Lutetia on 10 July 2010 with NASA´s Deep Space Network (DSN) 70-m antenna (DSS 63) near Madrid, Spain. Strong carrier signals at X-band (f_X=8.4 GHz) and S-band (f_S=2.3 GHz) were received throughout the flyby (Fig. S1) except for a planned tracking gap from 5 minutes before closest approach (t_0) to 40 minutes after t_0 and a short gap of 26 minutes starting at 192 minutes after t_0, when the uplink was accidentally dropped at DSS 63. The sampling time during the 10 hours of recording was one sample per second.

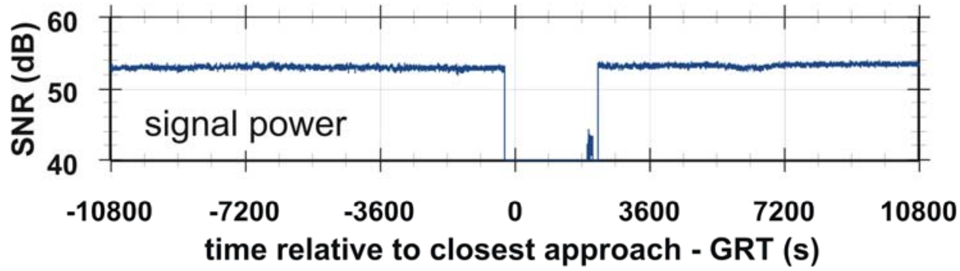

Fig. S1: Received signal power at X-band from Rosetta +/- 3 hours around closest approach.

2. Frequency Prediction

The received carrier frequency from the actual flyby is compared with a carrier frequency prediction of a spacecraft motion unperturbed by the asteroid. This frequency prediction is based on a complex force model taking into account gravitational forces (9) from the Sun and planets, and the largest asteroids Ceres, Pallas and Vesta, but not the target asteroid, and non-gravitational forces acting on the spacecraft (e.g. solar radiation pressure relative to a spacecraft macro-model with known optical parameters of each plane and the solar panels and their orientation at each time step). Also required are precise knowledge of the location of the ground station antenna phase center, and its behavior under forces like solid Earth tides and plate tectonic and a function of Earth rotation, precession and nutation (10). Relativistic propagation effects are considered up to second order (11).

The frequency prediction is routinely computed for radio science data processing on the Mars Express and Venus Express missions (12, 13).

3. Frequency residuals

The frequency shift from the perturbed spacecraft motion caused by the attracting force of the asteroid is extracted from the frequency recorded in the ground station on Earth by subtracting the predicted unperturbed frequency. The difference between the observed perturbed and the predicted unperturbed Doppler shift is the raw frequency residual (Fig. S2a).

Fig. S2 (next page): Frequency residuals at X-band from t_0-4 hours to t_0+6 hours. Two tracking gaps are indicated (light red shaded zones) from t_0-5 minutes to t_0+45 minutes as planned and from t_0+192 minutes to t_0+218 minutes when DSS 63 accidentally dropped the uplink. a) raw uncalibrated frequency residuals (observed frequency minus predicted frequency). These raw residuals must be corrected for tropospheric propagation (solid line). b) Frequency residuals after tropospheric correction. The feature between t_0+95 minutes and t_0+165 minutes was caused by an HGA slew in elevation and azimuth, thereby producing an additional velocity component along the line-of-sight. c) HGA slew rates in azimuth (red) and elevation (blue). It is evident that the HGA generated an additional Doppler shift at the highest slew rates, in particular starting at t_0-15 minutes. These contributions overcompensated the Doppler shift from the gravitational attraction of the asteroid. d) Frequency residuals corrected for the HGA slew rates. The large positive frequency residuals just before the first tracking gap are caused by the abrupt stop of the HGA slew. e) Filtered frequency residuals to reduce noise. The red solid line is a least- square fit to the data from which *GM* is determined.

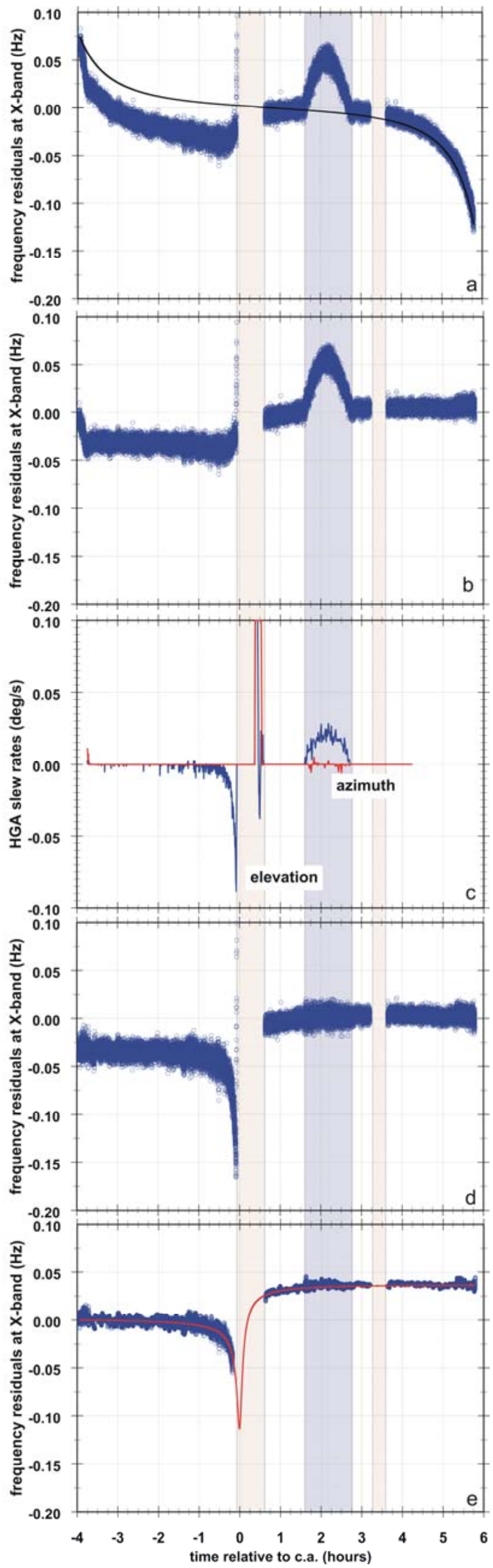
0.10
0.05
0.00
-0.05
-0.10
-0.15
-0.20
frequency residuals at X-band (Hz)
a
b
HGA slew rates (deg/s)
azimuth
elevation
c
d
e
-4
-3
-2
-1
0
1
2
3
4
5
6
time relative to c.a. (hours)

Fig. S2

4. Tropospheric correction

The raw frequency residuals during the flyby contain a contribution caused by the propagation of the radio signal through the Earth's troposphere. The propagation is mainly affected by the temperature, the atmospheric pressure and the partial pressure of water vapor. These meteorological parameters are recorded at the ground station site and used for calibration.

The tropospheric refraction of the radio ray path in the Earth atmosphere consists of two components: i) the dry component, the non-water-vapor component of the atmosphere, and ii) the contribution of the highly variable water vapor content of the atmosphere (the so-called wet component). The correction for refraction in the Earth's atmosphere is calculated with models for the path delay and mapping functions which project the path delay onto the direction of the signal path for the wet and dry components.

The models for the dry component (14), for the wet component (15), and the straightforward mapping functions (16) were used to compute the tropospheric correction. The uncertainty in the wet component is much larger than that of the dry component.

The tropospheric correction is subtracted from the raw frequency residual (Fig. S2a) to obtain the tropospherically corrected residual (Fig. S2b). The difference between three correction models (17-19) for the zenith delay and mapping functions was used to derive an systematic error estimate of the GM derivation.

5. *High Gain Antenna motion*

The steerable High Gain Antenna (HGA) of the spacecraft maintained Earth pointing until five minutes before closest approach, at which time the end position of the HGA motion was reached. The readjustment of the HGA resulted in a tracking gap of 45 minutes, including the time of closest approach. Pre-encounter flyby simulations, however, showed that stable and precise solutions for the mass can be achieved even with tracking gaps of several hours (7). While the Rosetta on-board instruments continued to track the asteroid, the HGA was articulated to reacquire Earth pointing. The varying HGA slew rates in azimuth and elevation (Fig. S2c) induced an extra Doppler shift along the line-of-sight (LOS), which began to become significant at 15 minutes before closest approach.

The rotation of the steerable HGA during the flyby induced an additional frequency shift on the observed radio signal which needs to be removed. This is done by applying the LOS component of $\Delta\boldsymbol{v} = \boldsymbol{\omega} \times \boldsymbol{r}$, where $\boldsymbol{r}$ is the vector from the center of mass (COM) to the phase center of the antenna and $\boldsymbol{\omega}$ the rotation rate of the antenna. Because the COM changed during the motion of the HGA, the location of the COM was adjusted during the fitting process.

To demonstrate this motion correction, we used a pre-planned HGA motion maneuver performed in 2004. The HGA was rotated from -95° to -23° in elevation with a maximum elevation rotation rate of 0.1°/sec and from -34° to 34° in azimuth with a maximum azimuth rotation rate of 0.03°/sec (Fig. S3). The maximum resulting frequency shift caused by the antenna rotation is about 300 mHz (Fig. S4). The frequency shift caused by the antenna motion was corrected by using the above model and the resulting residuals are shown in Fig. S5. It is seen that the frequency noise increased during the rotational motion caused by short term variations in the rotation rate. The additional frequency shift induced by the rotation of the HGA, however, is essentially removed from the frequency residuals, which are distributed about a mean value of zero.

The Doppler contributions from the HGA slew are evident in Fig. S2b. The increase in frequency shortly before closest approach contrasts with the expected (7) Doppler shift signature of the asteroid. The post-encounter feature between 95 min and 165 min is a specially designed spacecraft slew for Philae observations. The contributions from the HGA slewing motion are removed to obtain the frequency residuals in Fig. S2d, the calibrated and corrected Doppler shift caused by the asteroid between four hours before and six hours after closest approach.

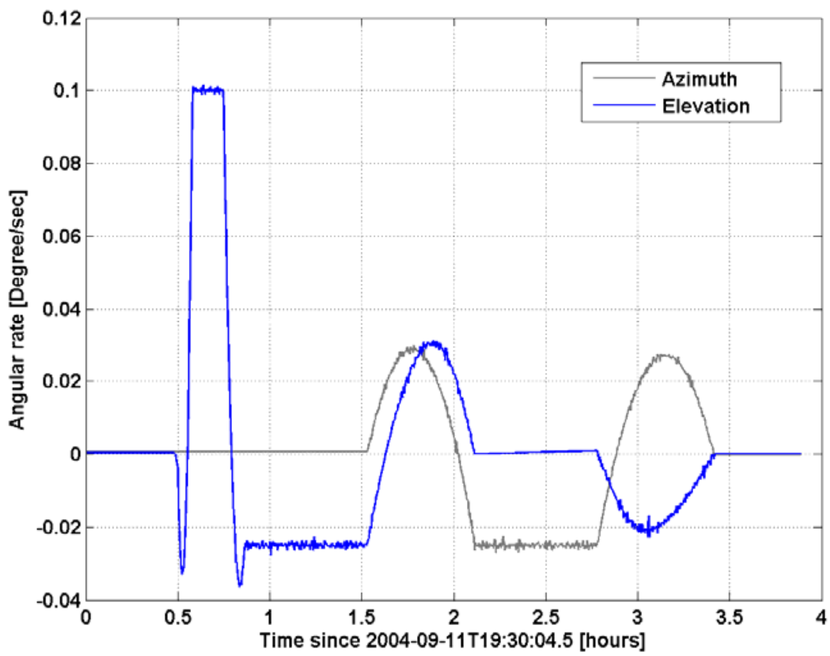

Fig. S3: Angular rates of the antenna motors in elevation and azimuth during a pre-planned maneuver in 2004. These values have been provided via the spacecraft housekeeping telemetry data.

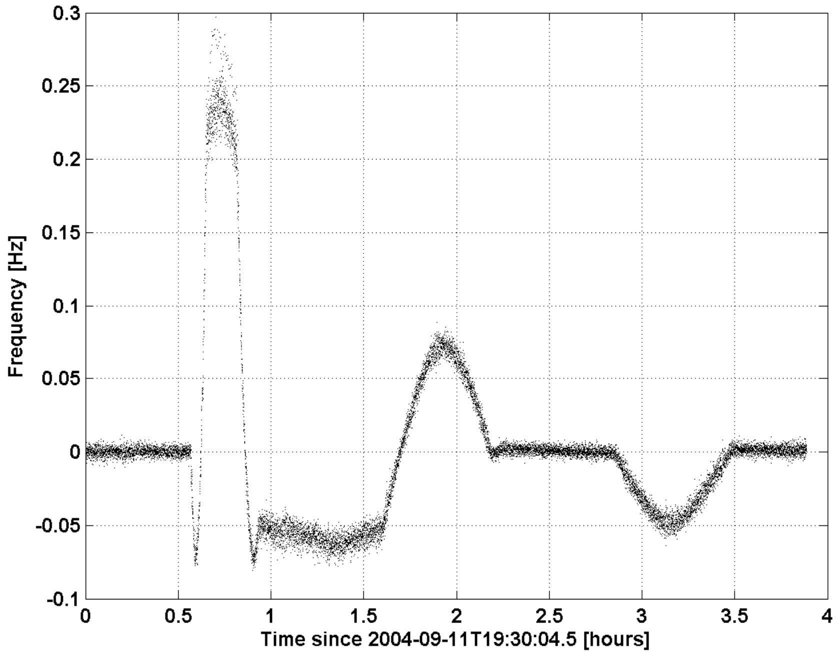

Fig. S4: Residual Doppler shift at X-band after subtracting the predicted frequency during the pre-planned maneuver in 2004. The large additional Doppel frequency shift is caused by the HGA motion in azimuth and elevation..

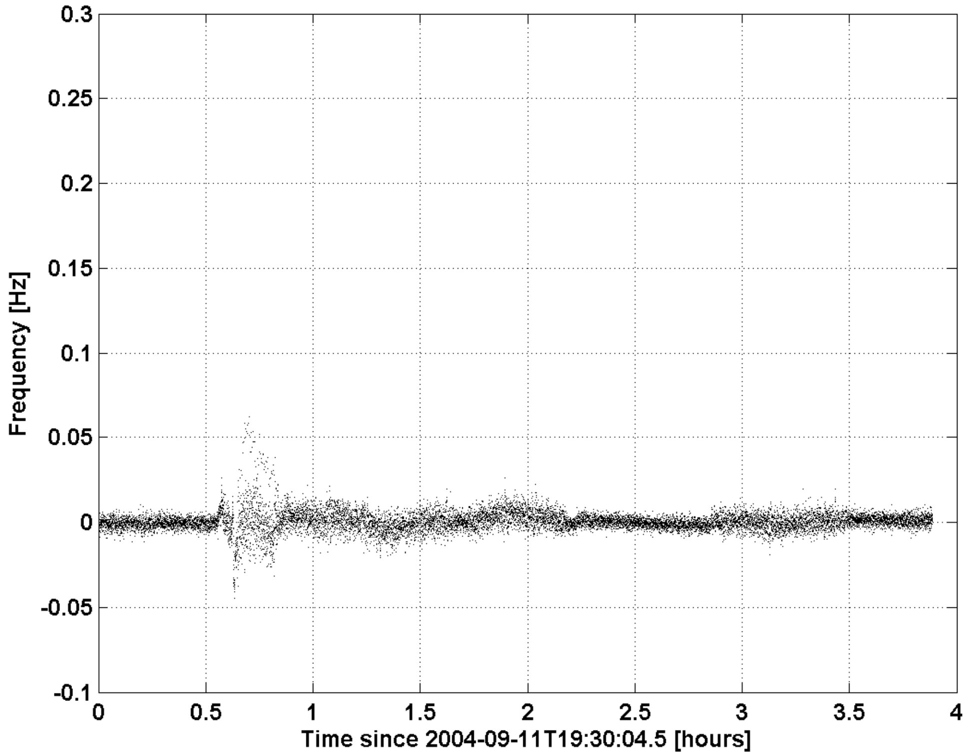

Fig. S5: Residual Doppler shift from the pre-planned maneuver in 2004 after correcting with the rotation rates of the HGA antenna motors in azimuth and elevation. The rotation rates and angles were provided via the spacecraft housekeeping telemetry data.

6. Filtering and adjustment

The frequency residuals in Fig. S2d were filtered at an integration time of 18 seconds for noise reduction.

Two different types of filters are used for data noise reduction: a Kaiser window filter and a moving average filter (20). Both filters are applied consecutively in forward and reverse direction ensuring a zero phase. The cut-off frequency f_c = 0.028 Hz Kaiser window filters and the integration time Δt = 18 seconds of the moving average filter were determined a priori with respect to the mass sensitivity. This approach avoids elimination of information in the data about the mass of the body and ensures that only noise is removed. The noise of the Lutetia flyby data was reduced in this step by more than a factor of two from 5.7 mHz to 2.6 mHz.

It is known from our experience with Mars Express and Venus Express radio science data processing that the frequency residuals can show a constant pre-event bias on the order of 10…50 mHz caused by contributions not considered in the prediction. In the Lutetia case, these contributions are not connected with the attracting force of the asteroid. The pre-encounter frequency residual bias of -32 mHz has been removed. This adjustment assumes a zero mean for the pre-encounter frequency residuals from t_0-4 hours to t_0-3 hours. The Hill sphere of influence of Lutetia (radius: 25,000 km) was entered at t_0-0.5h.

7. Fit and uncertainty

A least squares fit to the filtered curve (Fig. S2e) yields a solution for *GM*, an adjusted pre-encounter state vector, an adjusted solar radiation pressure constant and the scale factor for the motion of the HGA phase center with respect to the spacecraft center-of-mass.

The final Doppler frequency shift six hours after the closest approach is Δf = (36.2 +/- 0.2) mHz (Fig. S2e).

The mass and the other parameters were estimated with a weighted least-squares method. The initial velocity vector, the scale factor for the solar radiation pressure, the center of mass adjustment factor and the mass of Lutetia were fit using the frequency residuals. An initial state vector of the Rosetta spacecraft at t_0-4 hours is taken from the most actual SPICE-kernel[1] provided by the ESOC Flight Dynamics team as a first guess for the fitting procedure.

The change δx of the initial parameter set x iteratively aligning the measurement and the model is obtained from

$$\delta \boldsymbol{x} = (\boldsymbol{J}^T \boldsymbol{W} \boldsymbol{J} + \boldsymbol{I}\alpha)^{-1} \boldsymbol{J}^T \boldsymbol{W} \boldsymbol{\varepsilon},$$

where $\boldsymbol{J}$ is the Jacobi matrix, containing the partial derivatives of parameter set x, $\boldsymbol{W}$ the weighting matrix containing the standard deviation of the measurement, $\boldsymbol{\varepsilon}$ the difference between model and measurement, $\boldsymbol{I}$ the identity matrix and α is a damping factor. The damping factor serves as a numerical stabilization of the solution against ill-posed parameters (21). The iterative process is applied until the solution converges, i.e. measurement and models are aligned. The inverse of the term in parenthesis is computed using singular value decomposition (22).

The error of each parameter is derived from the diagonal terms of the covariance matrix

$$\boldsymbol{P} = (\boldsymbol{J}^T \boldsymbol{W} \boldsymbol{J})^{-1}.$$

The value of GM from the above described fitting procedure and considering further error sources is determined to be $GM = (11.34 \pm 0.11) \cdot 10^{-2}$ $km^3 s^{-2}$ corresponding to a mass of $(1.700 \pm 0.017) \cdot 10^{18}$ kg (error: 1.0%). The uncertainty

[1] The SPICE Kernel ORHR_______________00109.BSP is available from ssols01.esac.esa.int for all Rosetta experiment teams and is considered as a long term planning orbit file for experimental purposes.

in *GM* considers the error from the least squares fit mainly driven by the frequency noise (0.55%), the uncertainty in the Lutetia closest approach time introduced by the uncertainty in the flyby distance of +/-7.5 km (0.24%) and the considered uncertainty in the tropospheric correction introduced by the mapping function of the ground station elevation (0.8%) yielding a total uncertainty of 1.0%.

The post-fit Doppler residuals, the difference observation minus the fit are shown in Fig. S6.

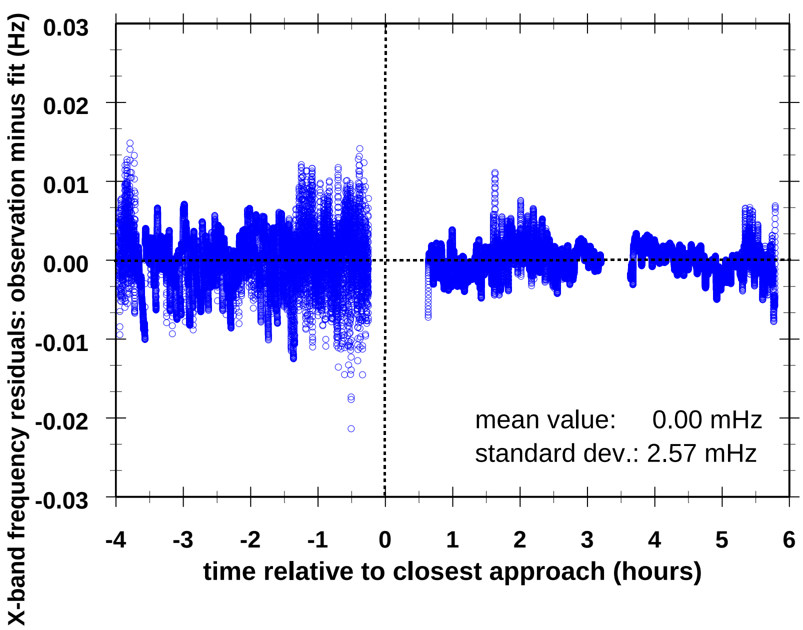

Fig. S6: Post-fit residuals after subtracting the least-squares fit from the filtered observation (Fig. S2e).

8. *Comparison with other mass determinations*

The mass estimate from the Rosetta flyby is compared in Fig. S7 with the asteroid masses derived from astrometry or perturbation calculations. The derived mass is lower than other mass determinations of Lutetia from astrometry (8, 23-25). A systematic bias is apparent: (26) derived a mass value of $(2.59 \pm 0.24)\cdot10^{18}$ kg for Lutetia from asteroid/asteroid perturbations, which is 70% larger and has an error of 15%. A more recent derivation (8) yields $(2.6\pm0.87)\cdot10^{18}$ kg where the error increased by a factor of 3. (23) derived a mass value of $(2.06 \pm 0.6)\cdot10^{18}$ kg from the influence of Lutetia on the motion of the planet Mars, which is 20% larger than (26) and has an uncertainty of 30%. Again, a more recent derivation (24) of $(2.55 \pm 2.34)\cdot10^{18}$ kg is closer to (22, 26) but has an error of 92%. The Jet Propulsion Laboratory (JPL) ephemeris DE421 (25) lists the mass of Lutetia as $(2.094 \pm 0.21)\cdot10^{18}$ kg with an error of 10%. Each precise direct mass determination of a large asteroid is therefore a valuable contribution to solar system dynamics.

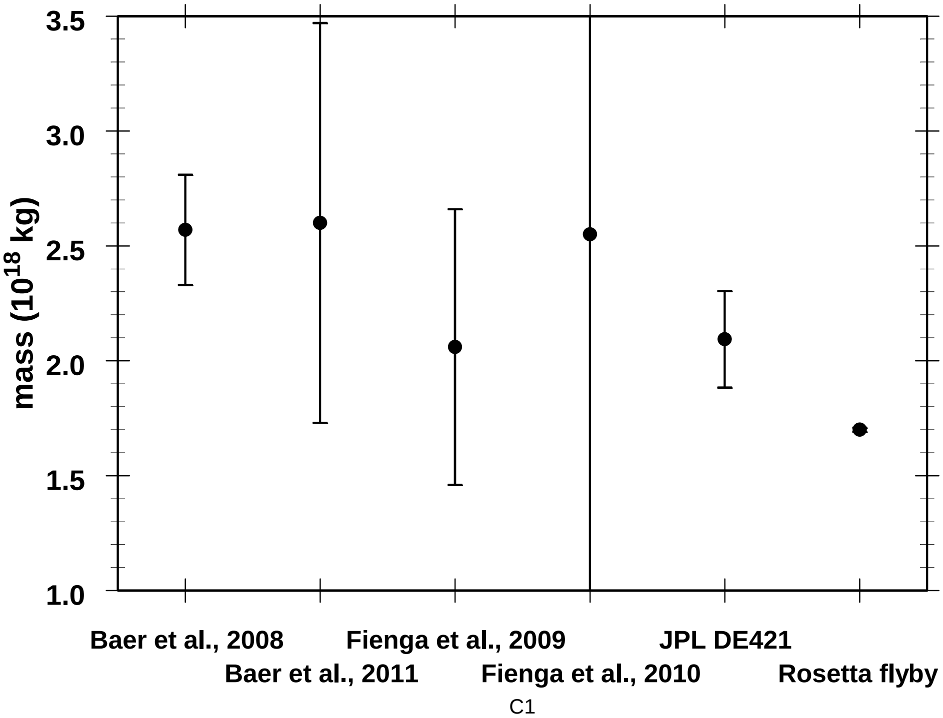

Fig. S7: Comparison between mass determinations of (21) Lutetia by astrometry (8, 24-26) and the Rosetta direct mass determination. The Rosetta error bar is smaller than the measurement point. The earlier derived values are systematically higher.

References and Notes

1. T. P. Andert *et al.*, *Geophys. Res. Lett.* **37**, L09202 (2010).
2. Materials and methods are available as supporting material on *Science* Online.
3. As shown in (*7*), the expected final post-encounter Doppler shift of a two-way radio carrier signal is $\Delta f(t \to \infty) = 4\frac{f_X}{c}\frac{GM}{d \cdot v_0} \cdot \sin\alpha' \cos\beta$, where $\alpha' = 172.18°$ is the direction to Earth projected into the flyby plane and $\beta = 3°$ is the direction angle to Earth above the flyby plane. Using the fit solution for Lutetia of $GM = (11.34 \pm 0.11) \times 10^{-2}$ km^3/s^2, the analytical result of the relation above is 36.4 ± 0.4 mHz.
4. H. Sierks *et al.*, *Science* **334**, 487 (2011).
5. Similar high bulk densities are known for the asteroids 4 Vesta, 16 Psyche, 20 Massalia, and 22 Kalliope, all of which are larger than Lutetia (*8*). Bulk

densities of more primitive C-type asteroids are in the range 1200 kg/m^3 to 2700 kg/m^3.

6. B. P. Weiss *et al*., Evidence for thermal metamorphism or partial differentiation of asteroid 21 Lutetia from Rosetta, paper no. 2077, 42nd Lunar and Planetary Science Conference, The Woodlands, TX, 7 to 11 March 2011.
7. M. Pätzold *et al*., *Astron. Astrophys.* **518**, L156 (2010).
8. J. Baer, S. R. Chesley, R. D. Matson, *Astron. J.* **141**, 143 (2011).
9. W. M. Folkner, J. G. Williams, D. H. Boggs, The Planetary and Lunar Ephemeris DE 421, IPN Progress Report 42-178, August 15 (2009); http://tmo.jpl.nasa.gov/progress_report/42-178/178C.pdf.
10. D. D. McCarthy, G. Petit, *IERS Technical Note* **N0**, 203 (2003); www.iers.org/nn_11216/IERS/EN/Publications/TechnicalNotes/tn32.html.
11. B. Häusler *et al*., *The Planetary Atmospheric Doppler Effect in a Relativistic Treatment*, Forschungsbericht, LRT 9-FB-5, 36 (Institut für Raumfahrttechnik, Fakultät für Luft- und Raumfahrttechnik, Universität der Bundeswehr München, 2007).
12. M. Pätzold *et al*., MaRS: Mars Express Radio Science Experiment, in *Mars Express: The Scientific Investigations*, ESA-SP 1291 (European Space Agency, Noordwijk, Netherlands, 2009), pp. 217–248.
13. B. Häusler *et al*., *Planet. Space Sci.* **54**, 1315 (2006).
14. J. Saastamoinen, Atmospheric Correction for the Troposphere and Stratosphere in Radio Ranging Satellites, in *The Use of Artificial Satellites for Geodesy*, S. W. Henriksen *et al*., Eds. (American Geophysical Union, Washington, D C, 1972), pp. 247–252.
15. I. Ifadis, The Atmospheric Delay of Radio Waves: Modeling the Elevation Dependence on a Global Scale, Technical Report no. 38L, School of Electrical and Computer Engineering, Chalmers University of Technology, Göteborg, Sweden, (1986).
16. C. C. Chao, A Model for Tropospheric Calibration from Daily Surface and Radiosonde Balloon Measurements, Technical Memorandum 391-350 (Jet Propulsion Laboratory, Pasadena, CA, USA, 1972).
17. T. Schüler, On Ground Based GPS Tropospheric Delay Estimation, PhD Thesis, Universität der Bundeswehr, München (2001).
18. J. Boehm, B. Werl, H. Schuh, *J. Geophys. Res.* **111**, (B2), B02406 (2006).
19. G. Petit, B. Luzum, IERS Conventions 2010 (International Earth Rotation and Reference Systems Service, 2010).
20. B. Buttkus, *Spectral Analysis and Filter Theory in Applied Geophysics* (Springer Verlag, Berlin, Heidelberg, 2000).
21. R. C. Aster, B. Borchers, C. Thurber, *Parameter Estimation and Inverse Problems* (Elsevier Academic Press, Amsterdam, 2005).

22. W. H. Press, S. A. Teukolsky, W. T. Vetterling, B. P. Flannery, *Numerical Recipes in Fortran* (Cambridge Univ. Press, Cambridge, 1986).

23. A. Fienga, H. Manche, J. Laskar, M. Gastineau, *Astron. Astrophys.* **477**, 315 (2008).

24. A. Fienga, H. Manche, P. Kuchynka, J. Laskar, M. Gastineau, Planetary and Lunar ephemerides, INPOP10A, arXiv.org > astro-ph > arXiv:1011.4419 (2010).

25. W. M. Folkner, J. G. Williams, D. H. Boggs, The Planetary and Lunar Ephemeris DE 421, JPL IOM, 343R-08-003 (2008); ftp://naif.jpl.nasa.gov/pub/naif/generic_kernels/spk/planets/de421_announcement.pdf.

26. J. Baer, S. Chesley, D. Britt, Eds., Asteroid masses V1.0 EAR-A-COMPIL-5-ASTMASS-V1.0, Nasa Planetary Data System (2009).